2. Yu AKF, Ng ASY. Complications and clinical outcomes of intraocular lens exchange in patients with calcified hydrogel lenses. J Cataract Refract Surg 2002; 28:1217–1222
3. Pandey SK, Werner L, Apple DJ, Kaskaloglu M. Hydrophilic acrylic intraocular lens optic and haptics opacification in a diabetic patient; bilateral case report and clinicopathologic correlation. Ophthalmology 2002; 109:2042–2051
4. Yu AKF, Kwan KYW, Chan DHY, Fong DYT. Clinical features of 46 eyes with calcified hydrogel intraocular lenses. J Cataract Refract Surg 2001; 27:1596–1606
5. Mamalis N. Complications of foldable intraocular lenses requiring explantation or secondary intervention—2001 survey update. J Cataract Refract Surg 2002; 28:2193–2201

because the lower eyelid laxity and levator disinsertion, the primary causes of involutional entropion, are not addressed by botulinum toxin injection.

In summary, botulinum toxin can effectively treat some cases of congenital entropion. It offers the ease of an in-office procedure and may obviate the need for surgical intervention.

REFERENCES

1. Bartley GB, Nerad JA, Kersten RC, et al. Congenital entropion with intact lower eyelid retractor insertion. Am J Ophthalmol 1991;112:437–441.
2. Yang LL, Lambert SR, Chapman J, et al. Congenital entropion and congenital corneal ulcer. Am J Ophthalmol 1996; 121:329–331.
3. Leblond E. Etiologie de le entropion congenital. Arch Ophtalmol 1907;27:782.
4. Tse DT, Anderson RL, Fratkin JD. Aponeurosis disinsertion in congenital entropion. Arch Ophthalmol 1983;101:436–440.
5. Steel DH, Hoh HB, Harrad RA, et al. Botulinum toxin for the temporary treatment of involutional lower lid entropion: A clinical and morphological study. Eye 1997;11:472–475.

Successful Treatment of Subfoveal Choroidal Neovascularization Associated With Combined Hamartoma of the Retina and Retinal Pigment Epithelium

Makoto Inoue, MD, Koushuke Noda, MD, Susumu Ishida, MD, Takefumi Yamaguchi, MD, Norihiro Nagai, MD, Kei Shinoda, MD, Hajime Shinoda, MD, and Yoshihisa Oguchi, MD

PURPOSE: To describe a patient with subfoveal choroidal neovascularization (CNV) associated with combined hamartoma of the retina and retinal pigment epithelium (CHRRPE), treated successfully by submacular surgery.

DESIGN: Interventional case report.

METHODS: A 12-year-old girl was referred to our clinic for evaluation. Visual acuity was 20/30 in the affected left eye. Ophthalmoscopy disclosed juxtapapillary CHRRPE and subfoveal pigmented CNV. Vitreous surgery was carried out because of visual deterioration to 20/60.

RESULTS: The posterior vitreous was strongly attached to glial tissue at the superior margin of the optic disk in the CHRRPE region. The CNV, which was not connected with the CHRRPE, was carefully removed, resulting in visual improvement to 20/20 5 months after surgery. Histologically, the excised membrane showed fibroblast-rich cellular component and a type 2 configuration.

CONCLUSION: Submacular surgery can be effective for the treatment of secondary CNV associated with CHRRPE. (Am J Ophthalmol 2004;138:155–156. © 2004 by Elsevier Inc. All rights reserved.)

Accepted for publication Feb 9, 2004.

From the Ophthalmology Department, Keio University School of Medicine, Tokyo, Japan.

Inquiries to Makoto Inoue, MD, Ophthalmology Department, Keio University School of Medicine, 35 Shinanomachi, Shinjyuku, Tokyo 160-8582, Japan; fax: (+81) 33359-8302; e-mail: inoshin@sc.itc.keio.ac.jp

COMBINED HAMARTOMAS OF THE RETINA AND RETINAL pigment epithelium (CHRRPE) are rare, benign tumors ophthalmoscopically observed as pigmented, slightly elevated lesions with retinal vascular tortuosity and epiretinal membranes.[1–3] Choroidal neovascularization (CNV) associated with these lesions may cause visual impairment.[1–3] Here we describe a patient with CHRRPE associated subfoveal CNV who was treated successfully by submacular surgery.

A 12-year-old girl was referred to us in December 2002 by a local ophthalmologist for further evaluation of retinal abnormalities in the left eye, in which she complained of decreased vision. Visual acuity deteriorated to 20/30 in the affected eye, compared with 20/20 at the most recent routine examination. Funduscopic examination revealed a pigmented tumorlike lesion at the superior margin of the optic disk, focal retinal vascular tortuosity, and subfoveal CNV (Figure 1, left). These findings were compatible with CHRRPE. Fluorescein angiography indicated hyperfluorescence at the subfoveal CNV, surrounded with hypofluorescence corresponding to the CHRRPE (Figure 1, right). Optical coherence tomography (OCT) showed a type 2 CNV, located between the sensory retina and the retinal pigment epithelium (RPE). Oral administration of prednisolone failed to improve vision and achieved no regression of subfoveal CNV, as evaluated by OCT. Exudative retinal detachment developed in the affected eye with visual deterioration to 20/60 3 months after the initial visit, which required vitreous surgery.

After core vitrectomy, posterior vitreous detachment was initiated by suction force using a vitreous cutter. However, the posterior vitreous cortex was attached strongly to the juxtapapillary CHRRPE. Subfoveal CNV was removed carefully with only slight bleeding and was not connected firmly to the juxtapapillary CHRRPE. A symptomatic scotoma affecting central vision was noted postoperatively but gradually decreased in size. Vision had recovered to 20/20 5 months after surgery, with complete regression of symptomatic scotoma (Figure 2, left). Histologic examination of the excised membrane showed fibroblast-rich cellular component, as well as extracellular matrix with capillary ingrowth (Figure 2, right). A layer of reactive RPE inverted onto the external aspect of the membrane represented a type 2 (subsensory retina) membrane.[4]

CHRRPE are typically detected at temporal macular or juxtapapillary sites in young adults; they are usually asymp-

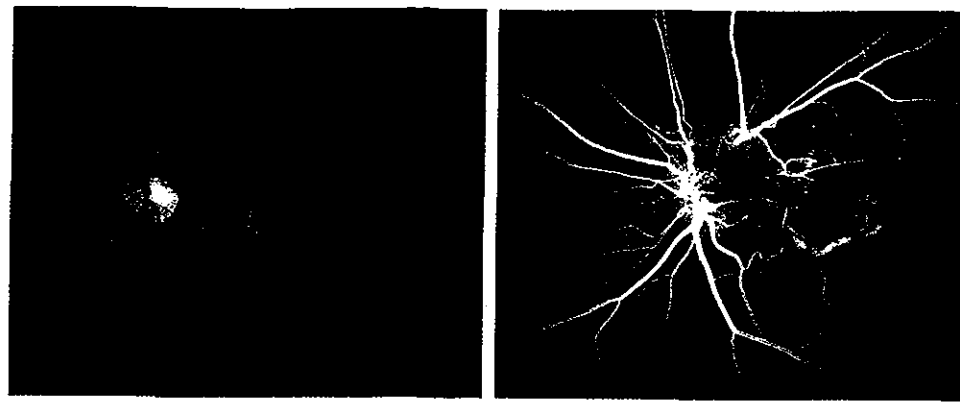

FIGURE 1. Left: Fundus photograph of the left eye indicating a pigmented tumorlike lesion at the superior margin of the optic disk associated with subfoveal choroidal neovascularization (CNV). Right: Fluorescein angiogram showing hyperfluorescence of the subfoveal CNV.

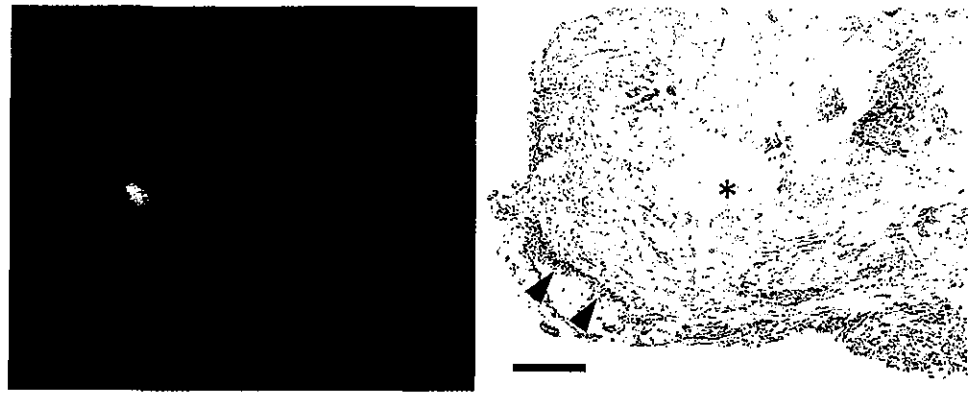

FIGURE 2. Left: Fundus photograph of the left eye 4 months after the surgery, showing successful removal of CNV with no recurrence. Right: Light microscopic photograph of the excised subretinal membrane. The asterisk indicates retinal pigment epithelium reflected onto its outer surface (arrowheads), representing a type 2 configuration (hematoxylin and eosin staining: bar = 200 μm).

tomatic, showing little change in size over time unless an epiretinal membrane or CNV develops.[1–3]

Although surgery has been attempted in cases of CHRRPE with retinal detachment, epiretinal membrane, or vitreous hemorrhage, visual outcomes were often unsatisfactory.[3] Reportedly, successful visual improvement following surgery was obtained when the hamartoma had been avulsed from the retina by vitreous traction in the course of posterior vitreous detachment.[5] Otherwise, successful surgical treatment for subfoveal CNV has not been described except for laser photocoagulation, which carries the risk of acute visual deterioration after treatment.[1–3] Photodynamic therapy is an alternative treatment for secondary subfoveal CNV, but visual improvement with this method would be limited because of subfoveal fibrosis. In our patient, the subfoveal RPE was relatively intact because the excised membrane had a type 2 configuration. Accordingly, submacular surgery can be considered a treatment option for secondary CNV associated with CHRRPE in selected cases.

REFERENCES

1. Yanoff M, Fine BS. Ocular pathology. 5th ed. St Louis: Mosby, 2002:660–663.
2. Gass JDM. Focal congenital anomalies of the retinal pigment epithelium. Eye 1989;3:1–18.
3. McDonald HR, Abrams GW, Bruke JM, et al. Clinicopathologic results of vitreous surgery for epiretinal membranes in patients with combined retinal and retinal pigment epithelial hamartomas. Am J Ophthalmol 1985;99:604–605.
4. Grossniklaus HE, Gass JDM. Clinicopathologic correlation of surgically excised type 1 and type 2 submacular choroidal neovascular membranes. Am J Ophthalmol 1998;126:59–69.
5. Holz FG, Alexandridis E, Volcker HE, et al. Spontaneous incomplete avulsion of juxtafoveal retinal pigment epithelial hamartoma. Arch Ophthalmol 2001;119:903–907.

Graefe's Arch Clin Exp Ophthalmol
(2004) 242:881–886

SHORT COMMUNICATION

DOI 10.1007/s00417-004-0908-9

Makoto Inoue
Kazuto Yamazaki
Kei Shinoda
Susumu Ishida
Hajime Shinoda
Kousuke Noda
Yoshihisa Oguchi

A clinicopathologic case report on macular hole associated with von Hippel–Lindau disease: a novel ultrastructural finding of wormlike, wavy tangles of filaments

Received: 18 October 2003
Revised: 27 February 2004
Accepted: 27 February 2004
Published online: 30 March 2004
© Springer-Verlag 2004

M. Inoue (✉) · K. Shinoda · S. Ishida · H. Shinoda · K. Noda · Y. Oguchi
Department of Ophthalmology,
Keio University,
35 Shinanomachi, Shinjuku-ku,
160-8582 Tokyo, Japan
e-mail: inoshin@sc.itc.keio.ac.jp
Tel.: +81-3-33531211 ext. 62402
Fax: +81-3-33598302

K. Yamazaki
Department of Pathology,
Saiseikai Central Hospital,
Tokyo, Japan

Abstract *Background:* We describe a novel ultrastructural finding observed in an epiretinal membrane excised from a patient with von Hippel–Lindau disease. *Methods:* This interventional case report presents a 45-year-old woman who noted decreased vision in her right eye and was referred for treatment of a macular hole secondary to von Hippel–Lindau disease. Blindness had occurred previously in the left eye because of exudative retinal detachment. Funduscopic examination revealed a macular hole associated with a delicate epiretinal membrane, multiple retinal angiomas, and multiple old laser scars. Vitrectomy was performed in her right eye. The epiretinal membrane was peeled off and processed for light and electron microscopy. *Results:* Postoperatively the macular hole was successfully closed, and vision recovered to 20/20 from 20/40. In the excised epiretinal membrane, flattened glial cells and extracellular matrix containing fibrous elements formed a multilayered pattern. Ultrastructurally, the fibrous elements appeared as wormlike, wavy tangles of filaments (WWTF) with an orientation parallel to the surface of the epiretinal membrane. Just above the WWTF, flattened glial cells frequently extended thin cytoplasmic processes with pinocytotic vesicles. *Conclusion:* The ultrastructure suggested that retinal glial cells had induced a remodeling of the collagenous stroma in the posterior vitreous cortex, resulting in tangential macular traction.

Introduction

Von Hippel–Lindau (VHL) disease was originally described as "angio-gliomatosis retino-cerebralis of Eugen von Hippel and Arid Lindau." Already in 1904, von Hippel pointed out the possibility of subjacent choroidal angiomas [18]. In 1962 and 1977, Schreck operatively and histopathologically found transscleral anastomoses of the retinal angiogliomas with posterior ciliary vessels [13, 14]. The multiple hemangiomas in the retina result in exudative retinal detachment, vitreous hemorrhage, neovascular glaucoma, and/or epiretinal membranes (ERM) [6, 19]. Multiple laser treatments are required to prevent leakage from retinal angiomas and subsequent exudative detachment. Despite such measures, the visual prognosis is unsatisfactory [6, 8, 19]. Macular hole associated with VHL disease is rare [5] and very little is known about the role of ERM in the development of the macular hole. To date, histological investigations have revealed that ERM play a key role in the development of vitreoretinal pathologies [2, 16]. However, detailed information to determine the clinicopathological implications of ERM associated with VHL disease is limited [6].

We present the case of a patient who underwent vitrectomy for a macular hole secondary to VHL disease. Vision recovered fully after successful closure of the macular hole. In an ERM excised from this patient, we encountered a novel ultrastructure in the newly synthesized extracellular matrix (ECM), which we termed wormlike, wavy tangles of filaments. This finding suggested abnormal remodeling of the collagenous stroma in

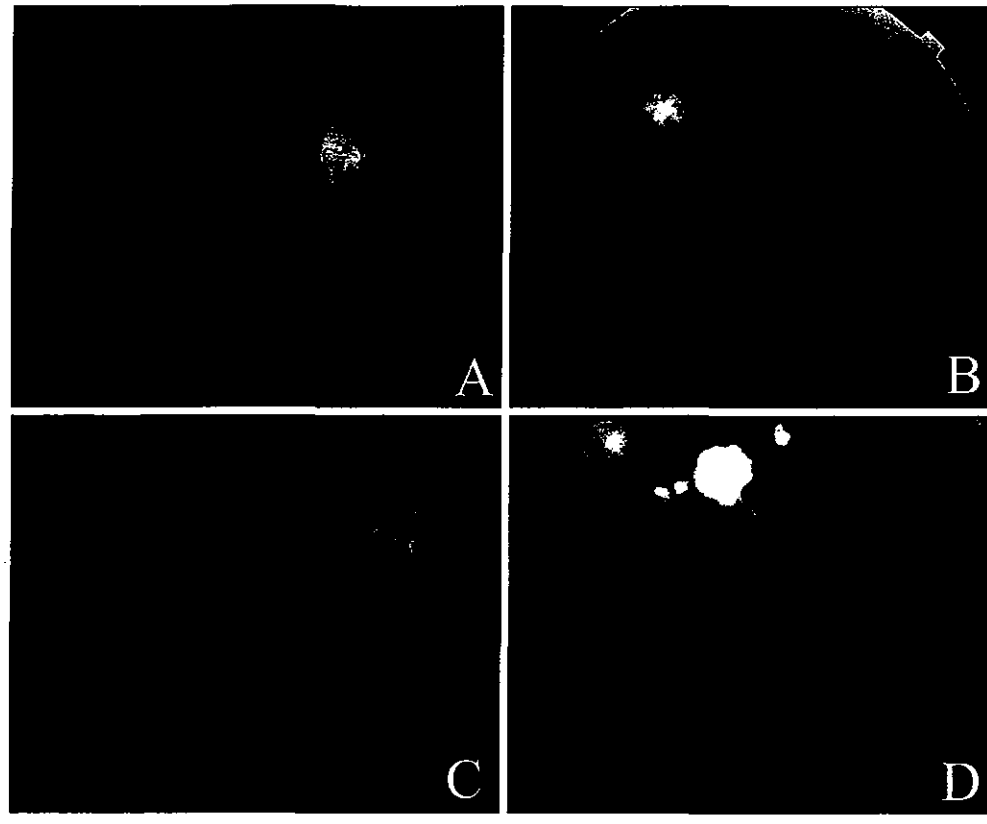

Fig. 1A–D Preoperative findings. **A** Photograph of the right eye. A macular hole with a yellow ring and eccentric retinal dehiscence and a delicate epiretinal membrane are seen. No pseudo-operculum is observed. Visual acuity was 20/40. **B** Photograph of the peripheral retina showing retinal angiomas. **C** A fluorescein angiogram at late phase shows hyperfluorescence in the macular hole, representing a window-defect pattern. **D** In the peripheral retina, a fluorescein angiogram showed hyperfluorescence in the retinal angiomas

the posterior cortical vitreous, which could cause retinal traction in VHL disease.

Material and methods

Clinical investigation

Ophthalmological examination of a patient who underwent vitrectomy for a macular hole associated with VHL disease included visual acuity, slit-lamp biomicroscopy, measurement of intraocular pressure, indirect ophthalmoscopy, fluorescein angiography, optical coherence tomography (OCT), and scanning laser ophthalmoscope (SLO) microperimetry.

Electron-microscopic analysis

The excised ERM was processed for light and electron microscopy. Briefly, a small sample of this tissue was fixed in phosphate-buffered 2.5% glutaraldehyde and processed routinely for embedding in epoxy resin. Ultrathin sections were stained with uranyl acetate and lead citrate and examined with an electron microscope, 1200 EX II (JEOL, Tokyo, Japan). The frequency of the membrane structure was evaluated using 42 electron micrographs at a magnification of ×4,000–6,000, with profiles of specialized structures being counted per unit length in the section image.

Results

Case report

A 45-year-old woman was referred to us in 2000 because of decreased vision in her right eye secondary to a macular hole associated with VHL disease. She had been followed up by a local physician for around 20 years after repeated laser treatments for retinal angiomas. She also had a history of renal angioma and cerebellar hemangioblastoma, which had been treated when she was 14 and 16 years old. Her left eye had been blinded by exudative retinal detachment about 20 years before the present referral.

Visual acuity was 20/40 in the right eye. Funduscopic examination revealed a macular hole associated with a delicate ERM and multiple peripheral retinal angiomas (Fig. 1A, B). The macular hole with a diameter of 200 μm, which showed a double-ring appearance of a yellow ring (outer ring) with eccentric retinal dehiscence (inner ring), but without premacular opacity, was considered to be a stage 2 hole according to the international classification by Gass. The optic disc was dragged toward an inferonasal laser scar. SLO perimetry detected an absolute scotoma of size 3 corresponding to the macular hole (the inner circle of retinal dehiscence), and the Watzke–Allen sign was present. The late phase of fluo-

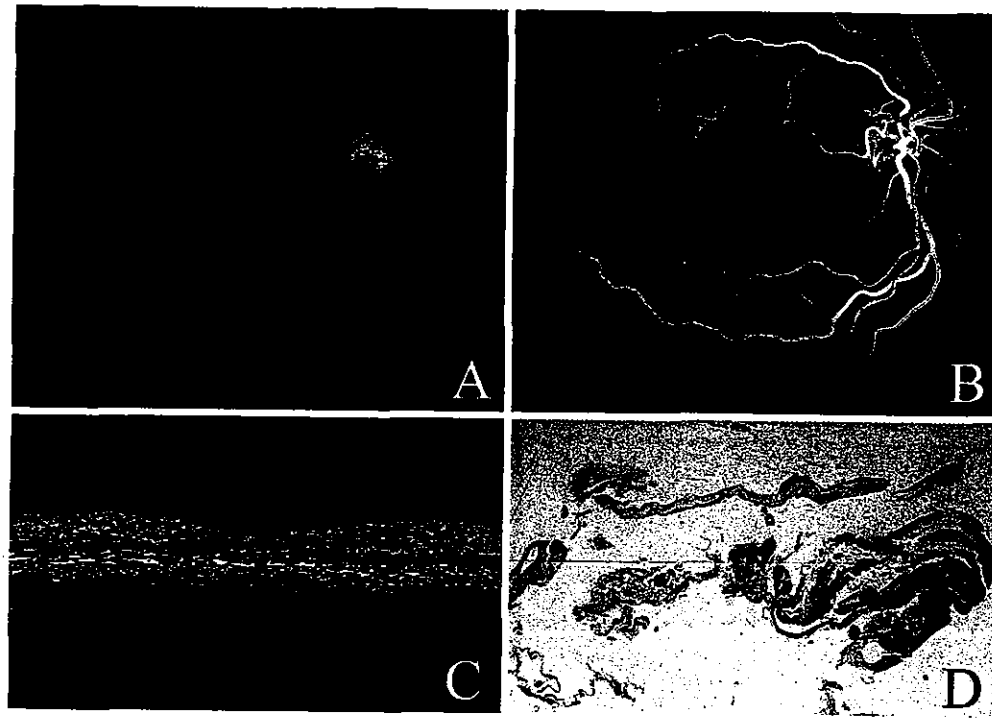

Fig. 2A–D Postoperative findings. **A** Photograph of the right eye. The epiretinal membrane has been peeled off, and the macular hole has closed. **B** A fluorescein angiogram showed decrease of hyperfluorescence at the macular hole. **C** Ocular coherence tomography: complete closure of the macular hole is confirmed. **D** Light microscopy of the excised epiretinal membrane, which consists of fibrous and cellular components. (toluidine blue; ×300)

rescein angiography showed hyperfluorescence in the macular hole (the outer yellow ring), representing a window-defect pattern (Fig. 1C). Peripheral angiomas also showed hyperfluorescence (Fig. 1D). Vitrectomy was performed in the patient's right eye.

Posterior vitreous detachment appeared to be present, while no glial ring was observed. After the gelatinous vitreous had been dissected away, the ERM was peeled off. Slight bleeding was then evident at the site of teleangiectasis, with vessels showing arteriovenous shunting at the superotemporal to the macula; this suggested that abnormal vasculature had been adherent to the ERM. Diathermy was applied to retinal angiomas [6], and 20% sulfur hexafluoride gas was injected for tamponade. The patient was instructed to maintain face-down position for a week.

The macular hole was closed successfully after surgery, and vision had recovered to 20/20 after 3 months (Fig. 2A). FA showed decrease of hyperfluorescence at the closed macular hole (Fig. 2B). Closure of macular hole was confirmed by the OCT findings and by disappearance of the Watzke–Allen sign (Fig. 2C). Vision remained at 20/20 for 2 years after surgery, with no signs of recurrence. Coagulated angiomas were observed to become smaller.

Electron-microscopic findings

Light microscopy of the ERM using toluidine blue staining of semi-thin sections showed fibrous and cellular components (Fig. 2D). Under the electron microscope, two to three layers of flattened glial cells alternated with fibrous matrix similar to findings in membranes excised from other ophthalmologic patients (Fig. 3A,B) [3, 12]. The ERM consisted of a fibrocellular array with flattened cells at the surface showing short microvillous cytoplasmic protrusions. Beneath the surface, collagen fibers formed a thick layer. Flattened glial cells and ECM containing fibrous elements were sandwiched to form a multilayered structure. Distinctive abnormal extracellular structures were apparent in the fibrous elements of the ERM (Fig. 3B–E).

The collagenous fibers, with diameters of approximately 11–20 nm (13.7±2.8 nm), took the form of worm-like, wavy tangles of filaments (WWTF) (Figs. 3B–E, 4). The WWTF had a central electron-dense core structure surrounded by bundles of fibers. The WWTF had a string-like or ropy structure with a diameter of approximately 200–300 nm and a length of 2–5 μm, running parallel to the surface of the ERM (Fig. 3B). Around the WWTF, matrix fibers were sparse compared with more distant portions of the ERM (Fig. 3B). The WWTF appeared frequently in the ECM just beneath the glial cells at the surface (Fig. 3B). Their frequency of occurrence was approximately 7.8 profiles of the WWTF per 2.5 μm of ERM section image based on 42 electron micrographs. Just above the WWTF, flattened glial cells frequently extended thin cytoplasmic processes with many small vesicles suggesting transporting activity (pinocytosis; Fig. 3B,D).

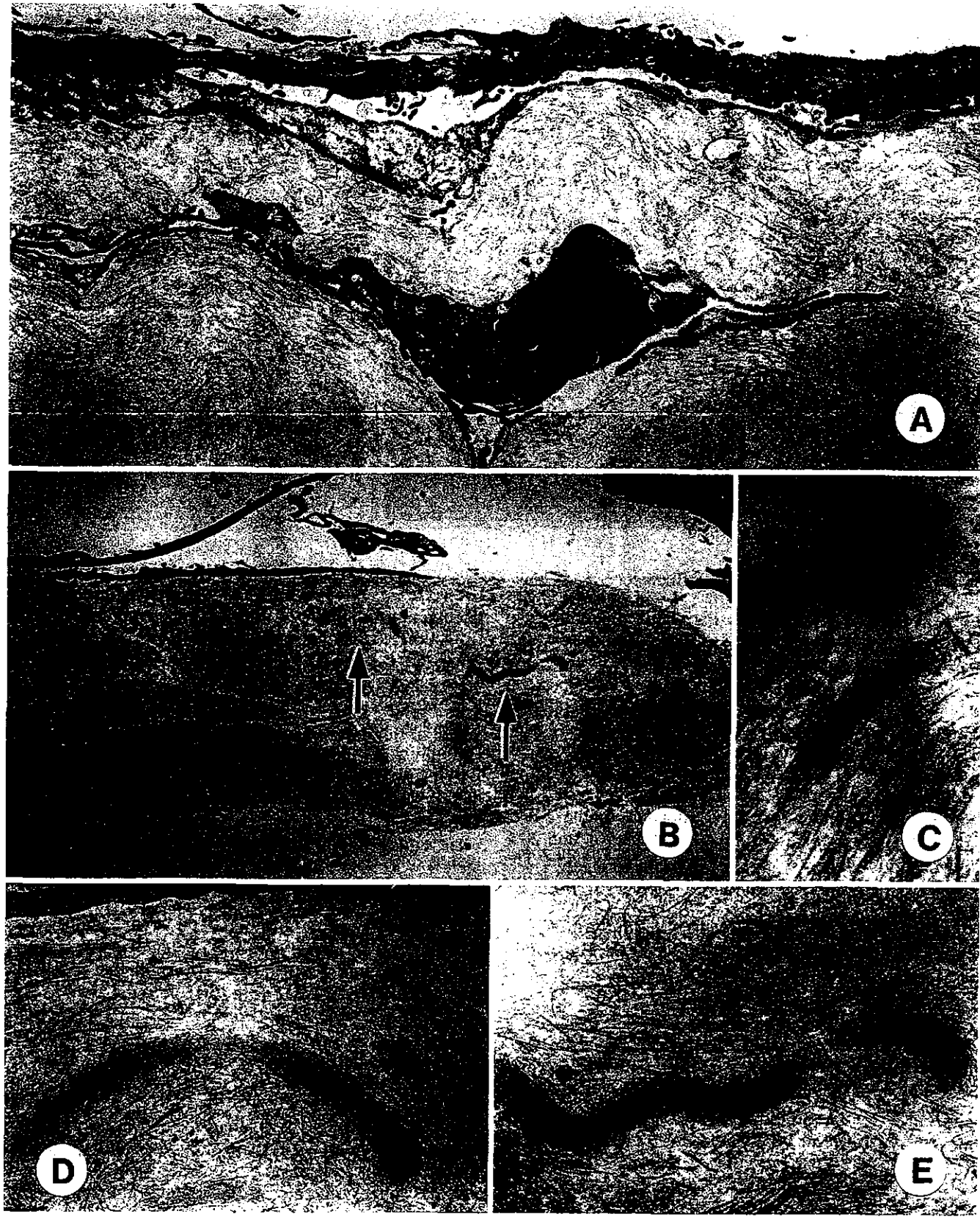
A
B
C
D
E

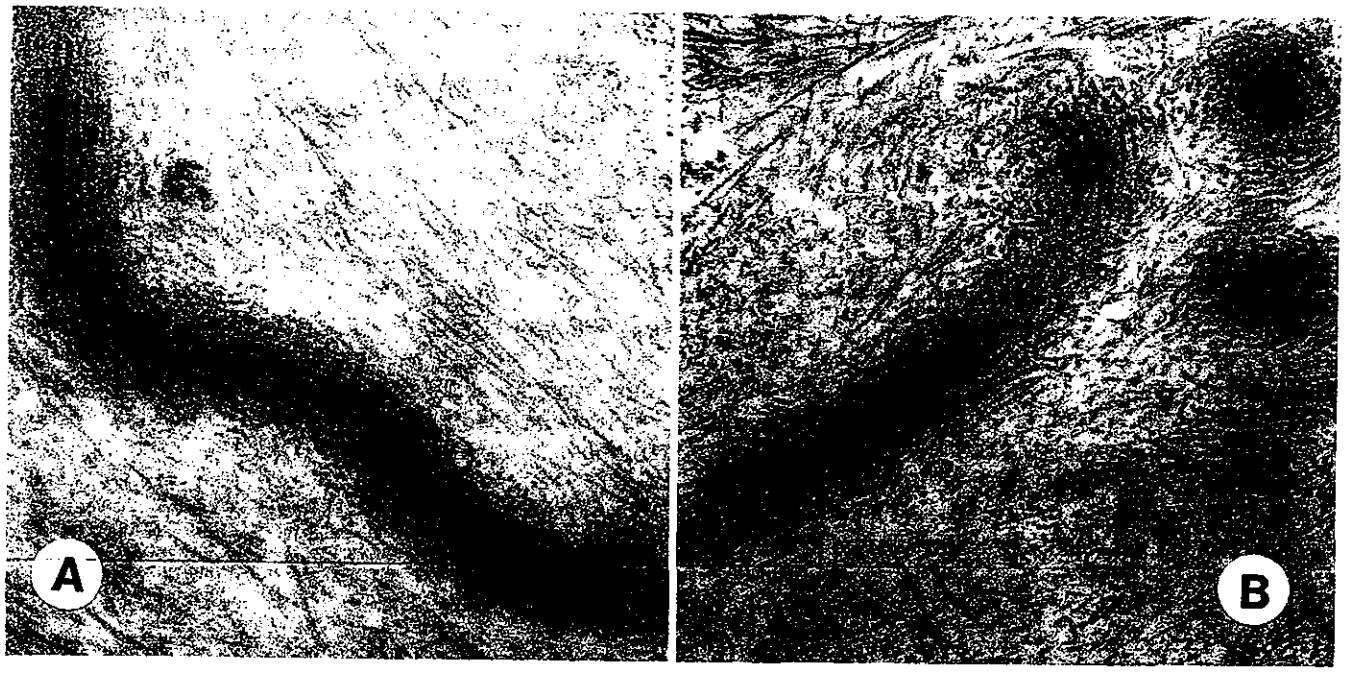

Fig. 4A, B Features at high magnification. **A** A longitudinal profile of WWTF shows central aggregates of fibers forming a dense core, surrounded by bundles of fibers (×52,000). **B** Oblique and transverse profiles of the WWTF shows differences from fibrous long-spacing collagen (×52,000)

Discussion

The current study shows a successful treatment of macular hole associated with VHL disease and a unique ultrastructural finding in the ERM removed during vitrectomy. In the literature, the visual prognosis of VHL disease is poor because of recurrent retinal angioma and exudative detachment [6, 18, 19]. Vitrectomy is an effective treatment for such retinal manifestations of VHL, particularly in the presence of massive exudative detachment that resists local laser treatment [5, 6, 8]. The mechanism by which vitrectomy alleviates exudative retinal detachment is unknown, but intravitreous transmission of subretinal fluid escaping through the retina may be facilitated by removal of the gelatinous vitreous gel [6].

Reported electron-microscopic findings of a retinal angioma in a VHL disease patient showed multiple layers of collagen matrix that indicated repeated exudation from retinal angiomas [9]. Few detailed histological observations have been presented concerning ERM removed from VHL patients [6]. The configuration of this ERM was quite similar to those in previous reports, that is, a layer of cortical vitreous with cells along its inner aspect [2, 16]. Since previously described new collagen in the vitreous typically had a fibril diameter of 25 nm or more [6], the present structures of the WWTF might be vitreous fibers with a central core of densely aggregated collagen fibrils and a surrounding zone of less densely aggregated fibrils within a loose matrix of collagen—with a diameter of 13.7±2.8 nm, similar to that of vitreous fibers [15]. The ultrastructure of vitreous fibers had been previously described to display a bundle of parallel fibers with a uniform diameter, but without a central core of aggregated fibrils [15].

The appearance of thick collagen fibers or fibrous long-spacing collagen (FLSC) has been considered indicative of cell-mediated remodeling of the ECM showing abnormal accumulations of FLSC in an ERM [1, 2, 16]. The WWTF are readily distinguished from FLSC. Even though the sparse type of FLSC may resemble tangentially cut profiles of the WWTF, the overall structure with an electron-dense core surrounded by bundles of wavy,

Fig. 3A–E Transmission electron photographs of the epiretinal membrane excised from a patient with von Hippel–Lindau disease. **A** The membrane consists of sandwiched layers of flattened glial cells and fibrous extracellular matrix (×7,200). **B** Just beneath a surface layer of flattened glial cells, aggregates of wormlike, wavy tangles of filaments (WWTF) are seen (*arrows*). Around these aggregates of the WWTF, matrix fibers are less plentiful than at a distance (see right and left sides; ×5,300). **C** A greater magnification of the WWTF showing them in longitudinal profile and in transverse section. Bundles of fibers are seen (×24,000). **D** Longitudinally, a bowlike curvilinear profile is seen, while a transverse section (*upper right*) shows an electron-dense core structure. Just above and near the WWTF, extended thin cytoplasmic processes of flattened glial cells are abundant (×24,000). **E** The wavy ropelike structure of the WWTF consists of bundles of extracellular fibers with an electron-dense core structure (×24,000)

thick collagen fibers is clearly different. In addition, the WWTF are unlikely to be an artifact of tissue processing for electron microscopy, since the bundles have not been seen in other similarly processed ERM and they appeared very frequently in this case.

The WWTF may reflect a specific sort of abnormal remodeling in ERM from VHL patients. Since ordinary matrix fibers were relatively sparse in the immediate area of the WWTF, the WWTF may be a product of ECM remodeling by glial cells. Furthermore, the WWTF appeared frequently in the ECM just beneath the glial cell surface, with the glial cells extending thin cytoplasmic processes containing pinocytotic vesicles, which again suggested active remodeling of ECM by glial cells in this ERM [2, 10, 17]. Abnormal glial cell function and abnormal ECM metabolism, especially involving fibronectin and type V collagen, have been reported in VHL disease [10, 11, 17]. Abnormal proteins produced from VHL genes and exudation from the vascular anomalies in VHL might perturb glial cell function to cause abnormal remodeling of the ERM, including aggregation or alteration of collagen fibers and basement membrane constituents to form the WWTF [4, 7, 20]. The WWTF in the ERM removed from our patient with VHL disease suggest that the abnormal remodeling of collagenous stroma is intimately involved to develop macular traction in the pathogenesis of macular hole formation in this disease.

Definitive evidence that the retinal glial cells induce abnormal remodeling of the collagenous stroma in the posterior vitreous cortex could not be provided by this ultrastructural study alone. Further studies are required to analyse the function of the WWTF in addition to their morphology.

Acknowledgements The authors would like to acknowledge the technical assistance of T. Nagai and K. Fujita with respect to electron microscopy. The authors received no financial support.

References

1. Ghadially F (1997) Ultrastructural pathology of the cell and matrix. Butterworth-Heinemann, Boston
2. Ishida, S, Yamazaki, K, Shinoda, K, et al (2000) Macular hole retinal detachment in highly myopic eyes: ultrastructure of surgically removed epiretinal membrane and clinicopathologic correlation. Retina 20:176–183
3. Kinouchi R, Hirokawa H, Miyokawa N, et al (2001) Immunohistochemical study of idiopathic and secondary epiretinal membrane. *Nippon* Ganka Gakkai Zasshi 105:673–681
4. Latha B, Ramakrishnan M, Jayaraman V, Babu M (1999) Physicochemical properties of extracellular matrix proteins in post-burn human granulation tissue. Comp Biochem Physiol B Biochem Mol Biol 124:241–249
5. Loewenstein J (1995) Bilateral macular holes in von Hippel–Lindau disease. Arch Ophthalmol 113:143–144
6. Machemer R, Williams JM Sr (1988) Pathogenesis and therapy of traction detachment in various retinal vascular diseases. Am J Ophthalmol 105:170–181
7. Marshall GE, Konstas AGP, Reid GG, et al (1994) Collagens in the aged human macula. Graefes Arch Clin Exp Ophthalmol 232:133–140
8. McDonald HR, Schatz H, Johnson RN, et al (1996) Vitrectomy in eyes with peripheral retinal angioma associated with traction macular detachment. Ophthalmology 103:329–335
9. Mottow-Lippa L, Tso MOM, Peyman GA, Chejfec G (1983) Von Hippel angiomatosis. A light, electron microscopic, and immunoperoxidase characterization. Ophthalmology 90:848–855
10. Oda Y, Kawahara E, Minamoto T, et al (1988) Immunohistochemical studies on the tissue localization of collagen types I, III, IV, V and VI in schwannomas. Correlation with ultrastructural features of the extracellular matrix. Virchows Arch B Cell Pathol Incl Mol Pathol 56:153–163
11. Ohh M, Yauch RL, Lonergan KM, et al (1998) The von Hippel–Lindau tumor suppressor protein is required for proper assembly of an extracellular fibronectin matrix. Mol Cell 1:959–968
12. Okada M, Ogino N, Matsumura M, et al (1995) Histological and immunohistochemical study of idiopathic epiretinal membrane. Ophthalmic Surg 27:118–128
13. Schreck E (1962) Phakomatosen und Sehorgan. Bericht über die Tagung bayerischer und österreicher Augenärzte, Vienna
14. Schreck E (1977) Differentiakdiagnose in der Ophthalmologie. Enke, Stuttgart
15. Sebag J, Balazs EA (1989) Morphology and ultrastructure of human vitreous fibers. Invest Ophthalmol Vis Sci 30:1867–1871
16. Shinoda K, Hirakata A, Hida T, et al (2000) Ultrastructural and immunohistochemical findings in five patients with vitreomacular traction syndrome. Retina 20:289–293
17. Swinscoe JC, Carlson EC (1995) Type II collagen is a major component of bovine retinal microvessel extracellular matrix. Microcirculation 2:253–265
18. Von Hippel E (1904) Über eine sehr seltene erkrankung der Netzhaut. Klinische Beobachtungen. Graefes Arch Ophthalmol 59:83
19. Wing GL, Weiter JJ, Kelly PJ, Albert DM, Gonder JR (1981) Von Hippel–Lindau disease: angiomatosis of the retina and central nervous system. Ophthalmology 88:1311–1314
20. Wykoff CC, Pugh CW, Maxwell PH, et al (2000) Identification of novel hypoxia dependent and independent target genes of the von Hippel–Lindau (VHL) tumor suppressor by mRNA differential expression profiling. *Oncogene* 19:6297–6305

Graefe's Arch Clin Exp Ophthalmol
(2004) 242:792–799

LABORATORY INVESTIGATION

DOI 10.1007/s00417-004-0935-6

Michael Völker
Kei Shinoda
Helmut Sachs
Helmut Gmeiner
Thorsten Schwarz
Konrad Kohler
Werner Inhoffen
Karl Ulrich Bartz-Schmidt
Eberhart Zrenner
Florian Gekeler

In vivo assessment of subretinally implanted microphotodiode arrays in cats by optical coherence tomography and fluorescein angiography

Received: 23 December 2003
Revised: 17 February 2004
Accepted: 26 March 2004
Published online: 4 June 2004
© Springer-Verlag 2004

M. Völker · K. Shinoda (✉) · H. Gmeiner · T. Schwarz · K. Kohler · W. Inhoffen · K. U. Bartz-Schmidt · E. Zrenner · F. Gekeler
University Eye Hospital,
Calwerstrasse 7/1, 72076 Tübingen,
Germany
e-mail: shinodak@uni.de
Tel.: +49-7071-2987074
Fax: +49-7071-295568

H. Sachs
University Eye Hospital,
Franz-Josef-Strauß-Allee 11,
93053 Regensburg, Germany

Abstract *Background:* Following multiple promising investigations into restoration of vision in degenerative retinal disease by implantation of a sub- or epiretinal prosthesis, the step to clinical use in humans is impending. In this study we intended to establish optical coherence tomography (OCT) and fluorescein angiography (FA) first in research animals for noninvasive assessment of the condition of the posterior pole of eyes after intraocular implant surgery. *Methods:* Three adult cats that had undergone subretinal implant surgery were evaluated by OCT and FA between 1 and 470 days postoperatively. Eight adult cats served as control. In addition histology was performed. *Results:* In all three cats OCT demonstrated stable positioning of the implants in the subretinal space during the complete examination period. Transient retinal edema was found in the early postoperative period but decreased during follow-up. The retina over the implants was well attached at all times in cats 1 and 2; however, in cat 3 localized retinal detachment was demonstrated. FA showed intact retinal vasculature over the subretinal implant in high detail without interference from choroidal background fluorescence. *Conclusions:* OCT and FA have been fruitfully applied to cats to assess the morphological and circulatory conditions of the neuroretina and of its interface with the subretinal implant. The techniques may therefore provide a tool for objective, noninvasive in vivo evaluation of eyes that have undergone subretinal implant surgery, both in research animals and in humans.

Introduction

Numerous efforts are currently under way to develop retinal prostheses to replace degenerated photoreceptors in diseases such as retinitis pigmentosa (RP) and age-related macular degeneration [1, 3, 6, 16, 17]. In these diseases epi- or subretinal implants are intended to electrically stimulate the remaining cell populations [7, 11, 14].

Several animal investigations [4, 12, 15, 17, 18] have reported the stable fixation of subretinal implants within the subretinal space (SRS), and no major undesired reactions such as cell proliferation, inflammation, or retention of subretinal fluid have been reported in various histological studies even after several years [9, 12, 15, 18]. Up to now, no objective morphological data in vivo about retinal tissue and its interface with the implant have been available. Adequate methods for such purposes are mandatory because effective signal transduction can only be achieved if close, stable contact is obtained between the implant and the neurosensory retina. Histological post mortem examinations, however, show inherent limitations.

The purpose of this study was to ascertain the feasibility of optical coherence tomography (OCT) and fluorescein angiography (FA) in animals to assess the biocompatibility of subretinally implanted microphotodiode arrays (MPDAs). We report stable fixation of the MPDA

in the SRS and tight contact between the MPDA and the retina by OCT, and intact retinal vasculature and circulation by FA.

Methods

Animals

Three healthy adult cats were examined by OCT on days 1, 8, 17, and 51 after subretinal surgery in cat 1, and on day 99 in cats 2 and 3. Additionally, cat 3 was examined on day 470. FA was performed on day 51 in cat 1 and on day 470 in cat 3. Eight age-matched adult cats were examined by OCT as control. All animal experiments adhered to the "Principles of laboratory animal care" (NIH publication No. 85–23, revised 1985), the OPRR Public Health Service Policy on the Humane Care and Use of Laboratory Animals (revised 1986), and the U.S. Animal Welfare Act, as amended, as well as the local commission for animal welfare.

Surgical procedure

Surgery was done under intubation narcosis (1.8% isoflurane) in the left eye with pupils dilated. The high reflectivity of the tapetum lucidum required no endoillumination, thereby enabling two-port vitrectomy. Two sclerotomies were made 6.0 mm posterior to the limbus. After partial vitrectomy between sclerotomy and area centralis, a 31-gauge cannula (Visitec, Sarasota, FL) was used to create a localized retinal bleb by injecting a small amount of balanced salt solution; the bleb was enlarged by injecting Healon (Pharmacia, Stockholm, Sweden). A 2.5-mm retinotomy was then made circumferentially at the temporal portion on the bleb. The MPDA was introduced into the vitreous cavity with an intravitreal end-gripping forceps. After the MPDA had been inserted through the retinotomy into the SRS, it was forwarded ca. 1 mm outside of the created bleb under the retina near the area centralis.

MPDA specifications

The subretinally implanted prototype of a MPDA consisted of 48 single photodiodes which were grouped in fours to stimulate the retina via 12 titanium nitrite electrodes. The device measured 50 µm in thickness and 2 mm in diameter; it was electrically active and functioning (for a description of similar devices see [19]).

Optical coherence tomography

After intramuscular anesthesia and pupil dilation, cats were placed in front of the Optical Coherence Tomograph (Zeiss-Humphrey, Dublin, CA; software version A 6.1, 1997) in a stereotactic apparatus which ensured mechanical stability of the animal. The principle of the OCT has been described previously [13]. The following tomographic images were obtained in all animals (Fig. 1a): (1) a long vertical scan of approximately 6 to 8 mm along the axis including the MPDA, the optic disc, and the retinotomy site, and (2) vertical and horizontal (orthogonal to the vertical) scans of approximately 4 mm length over the MPDA. A digital video image was taken to visualize the OCT scan's position on the retina. For measurements of the MPDA's diameter in horizontal direction the eye length was adjusted to 21.50 mm (manufacturer's recommendation).

Thickness and horizontal length measurements (in micrometers and millimeters, respectively) were performed using the instrument's built-in algorithm; accuracy of the automatic detection of the borders of the neurosensory retina was checked individually. The area comprised of the retina above the implanted MPDA was calculated by standard image-processing software which counted the number of pixels in the picture exported from the OCT software. To adjust for slightly differing scan lengths, mean retinal thickness was calculated by division of the area (in pixels×pixels) by the horizontal length in pixels and then transformed into micrometers. Mean retinal thickness was used to assess retinal tissue changes over time.

Fundus photography and fluorescein fundus angiography

FA was performed in the standard manner [5] with a fundus camera (TRC-50IA; TOPCON, Paramus, NJ). Photographs were taken with a black-and-white digital camera (Kodak Megaplus Model 1.4,

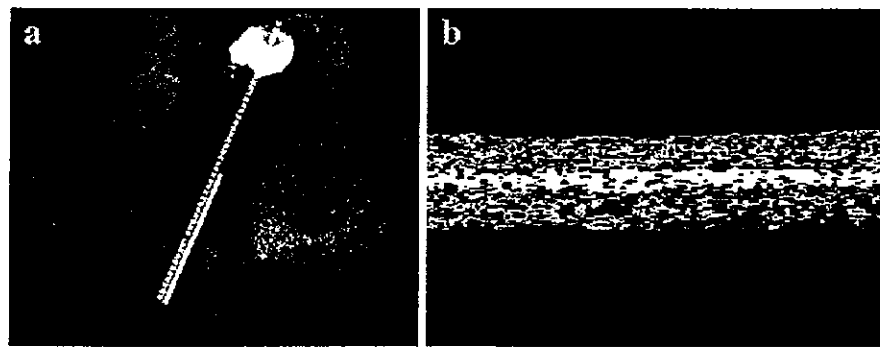

Fig. 1 **a** Black-and-white digital photograph with the three OCT scan paths (one long and two short scans) routinely used in all cats. Stable positioning of the microphotodiode array in the subretinal space near the area centralis is demonstrated. The retina appears attached in all areas. Peripherally from the microphotodiode array a black spot occurred in all cats in the area where the bleb had been formed during surgery to introduce the implant into the subretinal space. The area of high reflectance in the periphery of the black spot corresponds to the intentional retinal break exposing the cat's tapetum lucidum layer. **b** Illustrative horizontal OCT image of a control animal. The cat retina showed a more homogeneous structure than a human retina. The wider white band most possibly corresponds to the complex of tapetum lucidum and choriocapillaris

Eastman Kodak, Rochester, NY), after injection of 10 mg/kg of 10% fluorescein into a cephalic vein.

Histologic assessments of the retinae

After enucleation the anterior segment including the lens was removed and the posterior eye cups with the retina in place were fixed overnight at 4°C in 4% paraformaldehyde in 100 mM phosphate buffer, pH 7.4. Following the fixation a fine slit was made through the retina directly in front of the implant and the device was carefully removed out of its tissue pocket. The eye cup was then embedded in paraffin by standard protocols; radial 5-µm sections were cut, collected on slides, and examined microscopically after staining with hematoxylin and eosin.

Results

General remarks on OCT and FA imaging in cats

Due to the highly reflective tapetum lucidum, brightness ranges of the instrument had to be reduced to allow localization of the OCT beam on the video image. The OCT power and sensitivity had to be reduced by a factor of approximately 4. All other settings were comparable to those for human examinations.

One illustrative OCT image of a control animal is shown in Fig. 1b. In general, the cat retina had a more homogeneous appearance than the human retina where ideally the nerve fiber layer, the inner and outer plexiform layer, and the photoreceptor layer can be differentiated [13]. The subretinal layers in the cat showed much greater reflectivity than human eyes. The wider white band most possibly corresponds to the complex of retinal pigment epithelium (RPE), tapetum lucidum, and choriocapillaris. Mean retinal thickness of horizontal scans in the control animals was 215 µm±13.4 µm.

The highly reflective and intransmissible MPDA caused a total extinction of the OCT beam, inhibiting any evaluation of the structures behind the implant (e.g., Fig. 2).

Cat 1

Funduscopy revealed the MPDA in the desired position under the retina at all examination dates. The MPDA itself appeared intact. Neither persistent bleeding nor proliferative changes were observed at the posterior pole at any time. The retina appeared flat in all regions, including the area over the MPDA, except for small folds in the area where the bleb had been formed. The appearance of a black subretinal spot extending from the edge of the MPDA to the area where the bleb had been formed (Fig. 1a) did not alter over time. Localized retinal edema was suspected over the MPDA during the early postoperative period, although judgment of retinal alterations was made more difficult by the high reflectivity of the MPDA. Irregular retinal thickness was observed over the MPDA with a prominent thinning in the leading one third of the implant at all examination times.

On day 1 floating opacities in the vitreous cavity decreased the quality of fundus photographs, causing a low-reflection area behind them (Fig. 2). However, OCT images were obtainable. The retina over the MPDA was attached from day 1; it was detached in the area where the bleb had been formed but reached flatness also in this area on day 51 (Fig. 2). In the area of the black spot thinning of subretinal layers in OCT was observed (Fig. 2).

Irregular thickness of the neurosensory retina over the MPDA in the vertical scan was demonstrated; in the horizontal direction no such irregularity occurred (Fig. 2).

The range of the retinal thickness over the MPDA in the horizontal scan was 170–227 µm, 135–214 µm, 161–220 µm, and 136–175 µm on days 1, 8, 17, and 51, respectively. Mean retinal thickness was 195 µm, 190 µm, 195 µm, and 155 µm, respectively. Thickness in the vertical scan was 145–231 µm, 146–243 µm, and 110–214 µm on days 8, 17, and 51, respectively. Mean retinal thickness was 185 µm, 189 µm, and 161 µm, respectively. The development of mean retinal thickness above the MPDA is shown in Fig. 3.

FA on day 51 showed well-demarcated hypofluorescence corresponding to the MPDA and the black spot; at the border of the latter area also hyperfluorescence occurred. Otherwise no pathologic findings—such as leakage, neovascularization, or partial or total obstruction of vessels—were detectable (Fig. 4).

Cat 2

Funduscopy revealed an attached retina over the MPDA on day 1. In analogy to cat 1 we found an initial edema over the MPDA and a partial retinal thinning. On day 99 OCT scans showed retinal attachment over the MPDA (Fig. 5). Retinal conditions of the posterior pole including the site where the retinal bleb had been formed and the retinotomy site were comparable to cat 1. Retinal thickness over the MPDA ranged from 122 µm to 196 µm, corresponding to a mean retinal thickness of 163 µm (Fig. 3)

Cat 3

Funduscopy revealed no pathologic findings, in analogy to cats 1 and 2. On day 99 OCT scans of the retina over the MPDA showed a no-signal area between retina and MPDA extending over the central one third of the MPDA (Fig. 6). This may have corresponded to focal retinal detachment in this area that was not detectable by funduscopy. The retina in the area of the bleb was attached

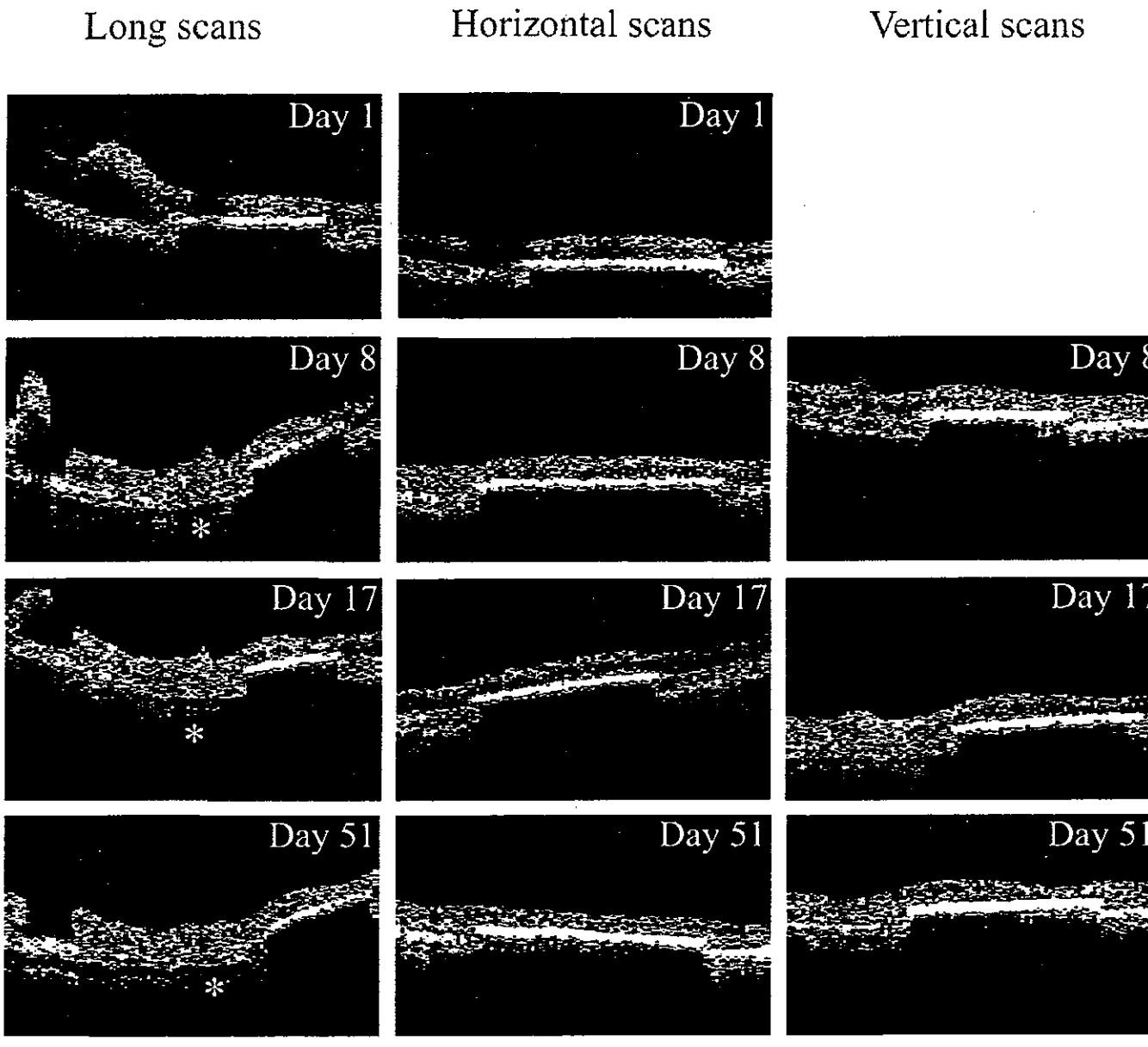

Fig. 2 OCT scans of cat 1 on days 1, 8, 17, and 51 (raw data). The *columns* show the different scan paths: vertical long scans of ca. 6–8 mm in the first column, detailed horizontal scans over the microphotodiode array of ca. 4 mm length in the second column, and detailed vertical scans of ca. 4 mm over the microphotodiode array in the third column. The *rows* show the scans at different time points. The subretinally implanted microphotodiode array, which is highly reflective and intransmissible, is observed as a homogeneously flat and white band with well-defined margins and homogeneous thickness, causing total extinction of the OCT beam, inhibiting any evaluation of the structures behind it. Retinal attachment over the microphotodiode array occurred on day 1. Low reflections located at a different position in the pictures in the first row were artifacts caused by vitreous opacities observed only in the early postoperative period. The irregularities in retinal thickness in the vertical scans which were not detectable in the horizontal scans decreased over the whole examination period. Retinal attachment has occurred in all areas at latest on day 51 in the area where the bleb has been formed during surgery and the area of the intentional retinal break. Thinning of subretinal layers appeared next to the implant in the area corresponding to the black spot seen in Fig. 1 (*)

(Fig. 6). Retinal thickness over the MPDA ranged from 95 µm to 190 µm, corresponding to a mean retinal thickness of 174 µm (Fig. 3).

On day 470 OCT scans of the retina over the MPDA still showed a no-signal area between retina and MPDA (Fig. 6). The retina in the area of the bleb remained (Fig. 6). Retinal thickness over the MPDA ranged from 98 µm to 184 µm, corresponding to a mean retinal thickness of 144 µm (Fig. 3).

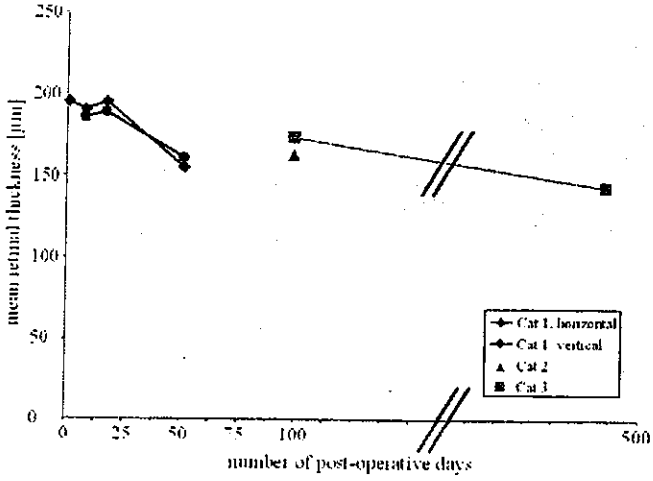

Fig. 3 Development of mean retinal thickness over time. In cat 1 mean retinal thickness over the implant decreased after an initial plateau of 17 days following surgery, in the vertical as well as in the horizontal scans. On day 99 mean retinal thickness over the implant in cats 2 and 3 was approximately the same as in cat 1 on day 51. In cat 3 mean retinal thickness further decreased between day 99 and day 470

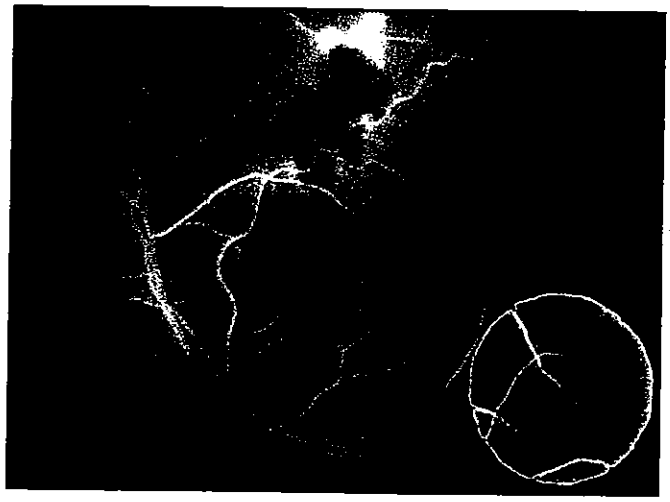

Fig. 4 Fluorescein angiography (FA) in cat 1 on day 51. The area over the microphotodiode array (*inset*) was photographed with different exposure time due to the high reflectance of the microphotodiode array. FA demonstrates no abnormal findings in the areas over the microphotodiode array and over the black spot, appearing in the area where the subretinal bleb was formed during surgery. Due to the blockage of background fluorescence by the microphotodiode array assessment of retinal vasculature was possible in high detail

In FA on day 470 no pathologic findings were detected, in analogy to cat 1, except a small area of hyperfluorescence at the upper border of the area where the bleb had been formed during surgery (Fig. 7).

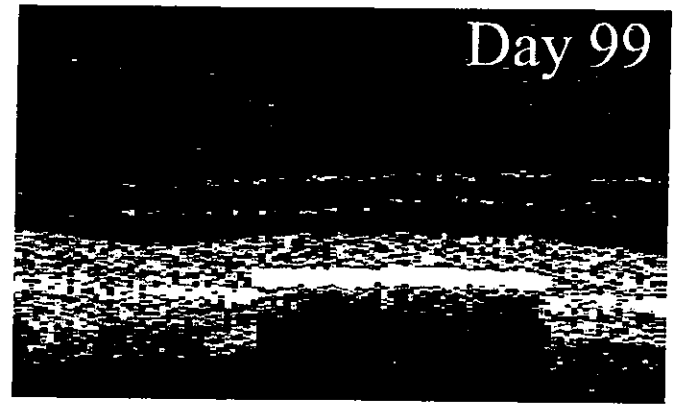

Fig. 5 OCT scans of cat 2 on day 99 (raw data). The retina over the microphotodiode array seemed totally attached and in close contact to the microphotodiode array. Two parallel lines in the vitreous cavity could correspond to the posterior vitreous cortex

Remarks on horizontal measurements of the MPDA by OCT

The MPDA's diameter ranged from 1.87 mm to 2.34 mm, corresponding to an under- or overestimation of 6.5% or 17%, respectively. Only 2 of 10 measurements were below 2 mm.

Surgical procedure

All surgeries were performed as planned with no serious adverse events resulting in stable positioning of the MPDA under the retina in the desired position. No complications (such as endophthalmitis and proliferative vitreoretinopathy) were observed during the follow-up period. Because of the anatomy of the cat eye's the following modifications to submacular surgery as practiced in humans were made: (1) only two sclerotomies were placed, (2) no posterior vitreous detachment (PVD) was created, (3) to maintain an opening for the introduction of the subretinal device into the retinal bleb viscoelastic material was introduced into the SRS, (4) from our previous experience no laser photocoagulation around the retinotomy was applied, (5) no tamponading substances, i.e., expanding gas or silicone oil, were used.

Histology

At 158 days postoperatively up to four rows of outer nuclear layer (ONL) cells were present in the retinal area overlying the implant along its margin. The number of these ONL cells decreased steadily from the margin towards the central regions of the implant, down to a single row of cells (Fig. 8a). The preservation of the inner retina varies, but the general retinal architecture was well pre-

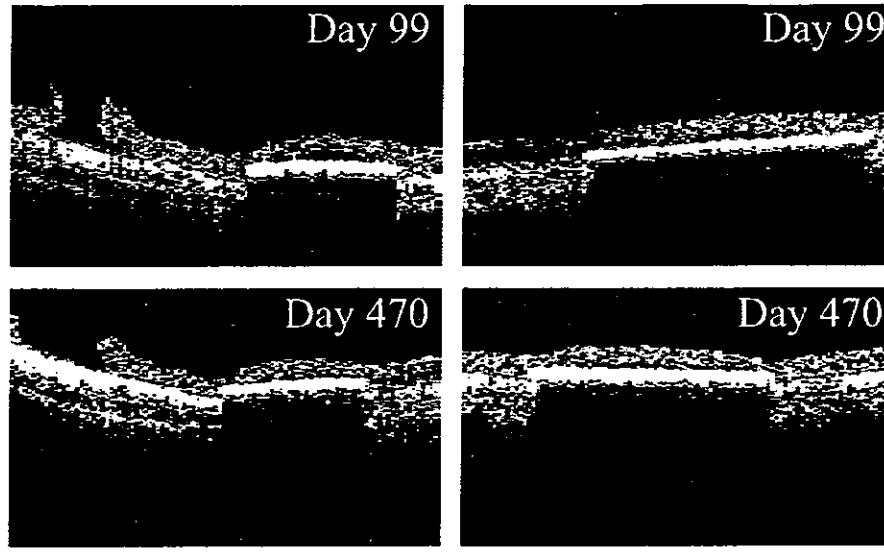

Fig. 6 OCT scans of cat 3 on days 99 and 470 (raw data). The *columns* show the different scan paths: vertical long scans of ca. 6–8 mm in the first column, detailed horizontal scans over the microphotodiode array of ca. 4 mm length in the second column. The *rows* show the scans at different time points. On day 99 the long scan demonstrates localized retinal detachment over the central one third of the microphotodiode array which is also visible in the horizontal scan. On day 470 this localized retinal detachment could still be observed, although to a lesser extent

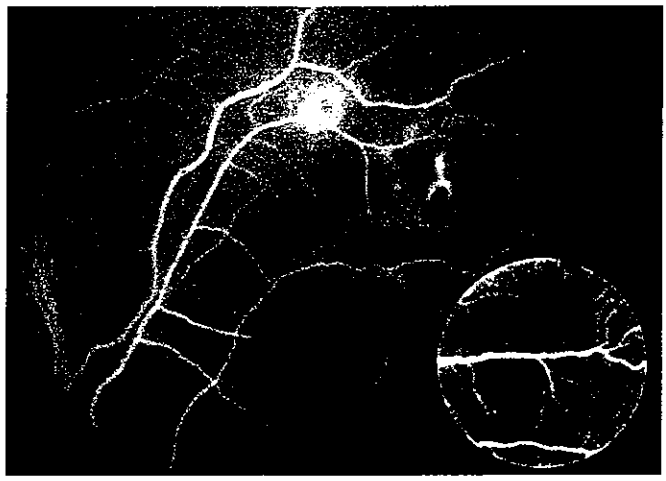

Fig. 7 Fluorescein angiography (FA) in cat 3 on day 470. FA demonstrates normal retinal vasculature in the posterior pole and in the area over the microphotodiode array (see *inset*)

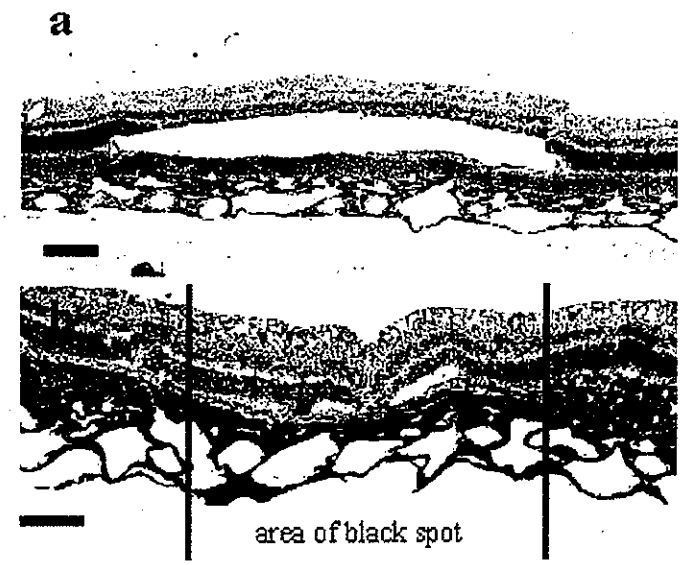

Fig. 8 Histological sections 158 days after implantation in cat 1. **a** The implant was removed prior to sectioning but its former position is clearly visible by a cavity located between the neurosensory retina and the retinal pigment epithelium/tapetum lucidum (*asterisk*). Note the well-preserved neuronal retina overlying the implant. **b** The black spot along the implantation channel where the tapetum lucidum has disappeared and the black-pigmented choroid is now located directly adjacent to the translucent retina. The tapetum lucidum laterally to the channel is marked by an *asterisk* (calibration bar is 200 μm)

served over the entire implant and the neuronal network of horizontal, amacrine, and ganglion cells was without substantial deficits. Hyperplasia of Müller glia was occasionally found, but minimal, in those areas where at least one row of ONL cells remained. The tissue bag surrounding the implant was coated with a fibrous membrane less than 10 μm thick.

Histology of the area of the black spot revealed a total loss of the tapetum lucidum (Fig. 8b). As a consequence

the pigmented choroid was visible in this area along the implantation channel.

Discussion

The feasibility of OCT examinations in cats which have undergone subretinal implant surgery using commercially available machines has been demonstrated successfully. This study provides to the authors' knowledge the first analysis of the cat fundus by OCT.

All images obtained were of superb quality without artifacts from foreign bodies as seen, for example, in computer tomography or ultrasound sonography. The possibility of performing OCT under these conditions might be of clinical importance in cases where localization or measurement of intraocular foreign bodies is required. Since the device totally blocked any imaging of details behind it, in the RPE or choroid OCT is applicable only to subretinal and not to epiretinal implants.

OCT imaging has several advantages over other imaging techniques and histological studies. First, it is noninvasive, thus allowing longitudinal studies. It can be applied to humans who have undergone subretinal implant surgery where stringent assessment of the retina over and around the device and of its stable positioning is of critical importance. Second, OCT is an in vivo technique, measuring tissue structures in living conditions, and it therefore does not suffer from artifactual changes in tissue morphology during histological preparation. Third, it is sufficiently sensitive to detect relatively small changes in retinal thickness. Fourth, OCT imaging is fast. Fifth, OCT images are digitized and are therefore objectively quantifiable for statistical analysis.

In cat 1 mean retinal thickness over the MPDA had decreased by day 51, suggesting resolution of postsurgical edema, and reached a level which was also found in cat 2 and cat 3 on day 99. This is in good accordance with observation by biomicroscopy and functional analyses where higher thresholds to elicit cortical responses following subretinal electrical stimulation were found in acute than in chronic experiments. Mean retinal thickness over the MPDA of cats 1–3 falls within the range of the control animals in the early postoperative period but falls outside during later examinations. The progressive thinning observed in all animals during the later stage is due to degeneration of outer segments which is proven by histology in Fig. 8, where an almost complete lack of this layer is demonstrated in contrast to a well-preserved inner retina. The deterioration of the photoreceptor layer, which is not vascularized, is due to the lack of nutrition from the underlying retinal pigment epithelium and choroid. As there is no debris found on either the front or the back surface of the implant an apoptotic mechanism seems to be most likely. Apoptotic cell death of photoreceptors has been described in degenerative retinal disease such as age-related macular degeneration.

In cat 1 retinal attachment over the MPDA's region was observed by OCT as early as day 1. It is speculated that the persistent subretinal fluid observed in cat 3 at all examinations is associated with lack of direct contact of this space with the RPE, with retention of, for example, the viscoelastic material over the MPDA, with the influence of the coating of the device, or with some tractional force of remaining vitreous cortex. Posterior vitreous cortex (as seen in Fig. 6) can be left undetected by OCT. In the current study creation of PVD was omitted due to strong attachment of the posterior vitreous cortex in the cat eye. Although successful submacular surgery without PVD creation has been reported in humans [8], strict removal of posterior vitreous can be considered important in the case of subretinal implantation in human eyes to prevent complications related to vitreous traction.

Irregularities in retinal thickness appeared in the long and vertical scans in cat 1 at all examination dates while not appearing in the horizontal scans. It might be associated with the physical force used while forwarding the MPDA within the SRS outside of the bleb.

OCT, in accordance with histology, showed no adverse tissue reactions such as cell proliferation or inflammation within the retina or around the implant in this study or in precursor studies [15]. This is in slight contrast to previous reports where cell proliferation, especially of Müller cells, has been demonstrated above and beneath the implanted device [10]. Differences, however, exist in animal models, surgical procedure, implant design and material, and method of histological preparation.

The slight variation of the horizontal length measurement from the actual size of the MPDA is attributed to off-center location of the examination beam. The overestimation of the MPDA's diameter by approximately 17% is attributed to the fact that the eye length was not individually assessed in our cats (instead, 21.5 mm was used).

Since MPDAs are totally intransmissible for the wavelengths used, FA can assess pure retinal circulation over subretinal implants to detect pathological conditions of retinal vasculature—ischemia, neovascularization, vasculitis, leakage, etc. FA in our animals demonstrated no abnormality of retinal vasculature, neither on day 51 nor on day 470. This finding further supports the assumption that the persistent subretinal fluid in cat 3 is associated with retained fluid rather than leakage from retinal vessels.

Black spots following subretinal surgery in cats have been previously reported [12]. Apparent thinning of subretinal layers in this area has been found by OCT in this study (e.g., Fig. 2). Histologically we were able to prove that the tapetum lucidum is absent or partially interrupted in this area, making the pigmented choroids visible through the unpigmented RPE. The alteration in

thickness of the highly reflective layer in the OCT image could provide in vivo proof of impairment of the tapetum lucidum, although OCT imaging of highly reflective layers is generally believed to be less reliable. Considering the fact that these spots were observed as soon as the first postoperative day, direct surgical trauma is a likely cause, although chemical injury by viscoelastic material cannot be excluded.

Since little experience has yet been gathered with subretinal implants in humans [2], much remains to be learned about the reaction of the (degenerated) human retina to subretinal implants. Certainly, the posterior pole of humans with implants has to be monitored closely, including not only the retina over the MPDA but also the site of the intentional retinal break and the area where the bleb has been formed during surgery. OCT so far provides the only noninvasive and objective technique to judge these conditions in humans over a prolonged period of time. In cases of implant failure evaluation of the retinal condition in regard to attachment to the MPDA, trauma, or edema can help to find the optimal treatment.

Acknowledgements Support of this study was provided by the Keio Gijuku Fukuzawa Memorial Fund for the Advancement of Education and Research and the German Federal Ministry of Education and Research (BMBF), grant 01 IN 502 A. The authors thank Chiaki Kato and Mitsuko Agarie for excellent technical advice. The collaboration with our partners in Stuttgart (IMS and IPE) and Reutlingen (NMI), who delivered the subretinal implants and were helpful in solving many technical problems, is appreciated.

References

1. Chow AY, Chow VY (1997) Subretinal electrical stimulation of the rabbit retina. Neurosci Lett 225:13–16
2. Chow AY, Packo KH, Pollack JS, Schuchard RA (2003) Subretinal artificial silicon retina microchip implantation in retinitis pigmentosa patients: long term follow-up. Invest Ophthalmol Vis Sci abstract, annual meeting
3. Eckhorn R, Stett A, Schanze T, Gekeler F, Schwahn H, Zrenner E, Wilms M, Eger M, Hesse L (2001) [Physiological functional evaluation of retinal implants in animal models]. Ophthalmologe 98:369–375
4. Gekeler F, Schwahn HN, Stett A, Kohler K, Zrenner E (2001) Subretinal microphotodiodes to replace photoreceptor-function—a review of the current state. In: Doly M, Droy M-T, Christen Y (eds) Vision, sensations et environnement, Irvinn, Paris, pp 77–95
5. Hill DW, Young S (1975) Infrared angiography of the cat fundus oculi. Arch Ophthalmol 93:131–133
6. Humayun MS, de Juan EJ, Weiland JD, Dagnelie G, Katona S, Greenberg R, Suzuki S (1999) Pattern electrical stimulation of the human retina. Vision Res 39:2569–2576
7. Humayun MS, Prince M, de Juan EJ, Barron Y, Moskowitz M, Klock IB, Milam AH (1999) Morphometric analysis of the extramacular retina from postmortem eyes with retinitis pigmentosa. Invest Ophthalmol Vis Sci 40:143–148
8. Kambara C, Inoda S, Shimizu Y, Tanabe K, Tuckwell HC (2000) [Optical coherence tomographic features after surgery for rhegmatogenous retinal detachment with macular involvement]. Jpn J Clin Ophthalmol 54:327–330
9. Kohler K, Hartmann JA, Werts D, Zrenner E (2001) [Histological studies of retinal degeneration and biocompatibility of subretinal implants]. Ophthalmologe 98:364-368
10. Loewenstein JI, Rizzo JF, Montezuma SR (2002) Implantation of subretinal polyimide in Yucatan pigs. Invest Ophthalmol Vis Sci abstract, annual meeting
11. Milam AH, Li ZY, Fariss RN (1998) Histopathology of the human retina in retinitis pigmentosa. Prog Retin Eye Res 17:175–205
12. Pardue MT, Stubbs EB, Jr., Perlman JI, Narfstrom K, Chow AY, Peachey NS (2001) Immunohistochemical studies of the retina following long-term implantation with subretinal microphotodiode arrays. Exp Eye Res 73:333–343
13. Puliafito CA, Hee MR, Lin CP, Reichel E, Schuman JS, Duker JS, Izatt JA, Swanson EA, Fujimoto JG (1995) Imaging of macular diseases with optical coherence tomography. Ophthalmology 102:217–229
14. Santos A, Humayun MS, de Juan EJ, Greenburg RJ, Marsh MJ, Klock IB, Milam AH (1997) Preservation of the inner retina in retinitis pigmentosa. A morphometric analysis. Arch Ophthalmol 115:511–515
15. Schwahn HN, Gekeler F, Kohler K, Kobuch K, Sachs HG, Schulmeyer F, Jakob W, Gabel VP, Zrenner E (2001) Studies on the feasibility of a subretinal visual prosthesis: data from Yucatan micropig and rabbit. Graefes Arch Clin Exp Ophthalmol 239:961–967
16. Wyatt J, Rizzo JF (1996) Ocular implants for the blind. IEEE Spectrum 33:47–53
17. Zrenner E (2002) Will retinal implants restore vision? Science 295:1022–1025
18. Zrenner E, Stett A, Weiss S, Aramant RB, Guenther E, Kohler K, Miliczek K-D, Seiler MJ, Haemmerle H (1999) Can subretinal microphotodiodes successfully replace degenerated photoreceptors? Vision Res 39:2555–2567
19. Zrenner E, Gekeler F, Gabel VP, Graf HG, Graf M, Guenther E, Haemmerle H, Hoefflinger B, Kobuch K, Kohler K, Nisch W, Sachs H, Schlosshauer B, Schubert M, Schwahn H, Stelzle M, Stett A, Troeger B, Weiss S (2001) [Subretinal microphotodiode array as replacement for degenerated photoreceptors?]. Ophthalmologe 98:357–363

Treatment of Retinal Detachment after Macular Translocation with Scleral Infolding: Preservation of Macular Translocation

Makoto Inoue, MD, Kei Shinoda, MD, Susumu Ishida, MD, Hajime Shinoda, MD, Norihiro Nagai, MD, Kousuke Noda, MD & Yoshihisa Oguchi MD

Reprinted from Retina, December 2004, Volume 24, Number 6

Brief Reports

TREATMENT OF RETINAL DETACHMENT AFTER MACULAR TRANSLOCATION WITH SCLERAL INFOLDING: PRESERVATION OF MACULAR TRANSLOCATION

MAKOTO INOUE, MD,
KEI SHINODA, MD,
SUSUMU ISHIDA, MD,
HAJIME SHINODA, MD,
NORIHIRO NAGAI, MD,
KOUSUKE NODA, MD,
YOSHIHISA OGUCHI, MD

From the Department of Ophthalmology, Keio University, Tokyo, Japan.

Limited macular translocation is an effective surgical procedure for subfoveal choroidal neovascularization (CNV) of less than one disk diameter without requiring large retinotomies.[1-4] However, various postoperative complications after limited macular translocation have been reported including retinal detachment (RD), macular holes, macular folds, and recurrence of CNV.[5,6] Treatment for such RD has not been well described in terms of preserving the translocation, except management for postoperative macular folds with intravitreal gas tamponade and release of scleral infolding suture.[7] Repairing RD after limited macular translocation leads to possible macular reattachment onto the original CNV site, limiting the increase in postoperative vision. Indeed, poor visual prognosis has been reported after the treatment for RD after limited macular translocation.[5]

Macular translocation with scleral infolding (MTSI) with absorbable suture was reported as one of variations of surgical procedures of limited macular translocation to provide regression of induced postoperative corneal astigmatism while keeping the distance of translocation after resolution of the scleral infolding.[4] We describe a new method for treating RD without a sign of proliferative vitreoretinopathy after MTSI preserving macular displacement by "transrelocation" of the macula.

The authors received no financial support.

Reprint requests: Makoto Inoue, MD, Department of Ophthalmology, Keio University, 35 Shinanomachi, Shinjyuku, Tokyo 160-8582, Japan; e-mail: noshin@sc.itc.keio.ac.jp

Case Reports

Case 1

A 63-year-old man had decreased vision in his right eye. Examination showed a visual acuity of 20/200 with subfoveal choroidal neovascularization of 0.8 disk diameter with Type 2 configuration, secondary to highly myopic degeneration (Figure 1). He underwent MTSI with absorbable suture[4] combined with removal of subfoveal CNV. The single intentional break to induce retinal bleb and remove subfoveal CNV was created near the superior arcade vessels, which was treated by laser photocoagulation postoperatively after absorption of intravitreal gas. One month later, visual acuity recovered to 20/40. Examination 2 months after MTSI revealed a decrease in vision to hand motion and total RD resulting from reopening of the intentional retinal break. Scleral infolding was observed to be still apparent. One milliliter of sulfur hexafluoride (SF_6) gas was injected intravitreally. Subsequently the patient was instructed to be lying with the affected eye downward for 30 minutes to start positioning, slowly elevated into an upright position for 1 hour, and then to be in a head-down position overnight. This procedure enabled inferior displacement of the macula with transient reattachment of almost the entire retina. The following day, perfluorocarbon liquid was injected at the start of surgery to keep the posterior retina from detaching. A small amount of subretinal fluid remained at the periphery, which was drained through the previous intentional break. No additional retinal break was found, except for the preexistent intentional break. Following repeat endophotocoagulation for the intentional retinal break, the eye was filled with 20% SF_6 gas. The retina was completely reattached with the macula transrelocated successfully with a shift of 1,500 μm, which was greater than the post-MTSI distance of 1,190 μm. The distance between the fovea and the border of CNV after the surgery was 870 μm, which was also greater than the post-MTSI distance of 790 μm. Vision recovered to 20/200 postoperatively 3 months after surgery and remained for 2 years.

Case 2

A 69-year-old woman had decreased vision in her left eye. Examination showed a visual acuity of 20/200 in the affected eye with subfoveal CNV of 0.4 disk diameter with Type 2 configuration, secondary to highly myopic degeneration (Figure 2). She underwent MTSI with absorbable suture without removal of CNV.

RETINA®, The Journal of Retinal and Vitreous Diseases, encourages authors to submit **Brief Reports** describing unusual findings, new techniques, and new instruments. Material submitted for consideration in this section of the journal is done so with the assumption that the data provided do not duplicate previously published material and that the material has not been submitted for consideration elsewhere. Each author must sign a disclosure to this effect (see Instructions to Authors for complete wording of transfer letter). Brief Reports submitted for this section of the journal may be subjected to the standard review process that is applied to other material submitted to **RETINA®**. Brief Reports should follow the requirements listed in the Instructions to Authors, with the following caveats: Brief Reports should not exceed 4 pages in length; no more than 5 references should be cited; and each Brief Report should include no more than 4 figures.

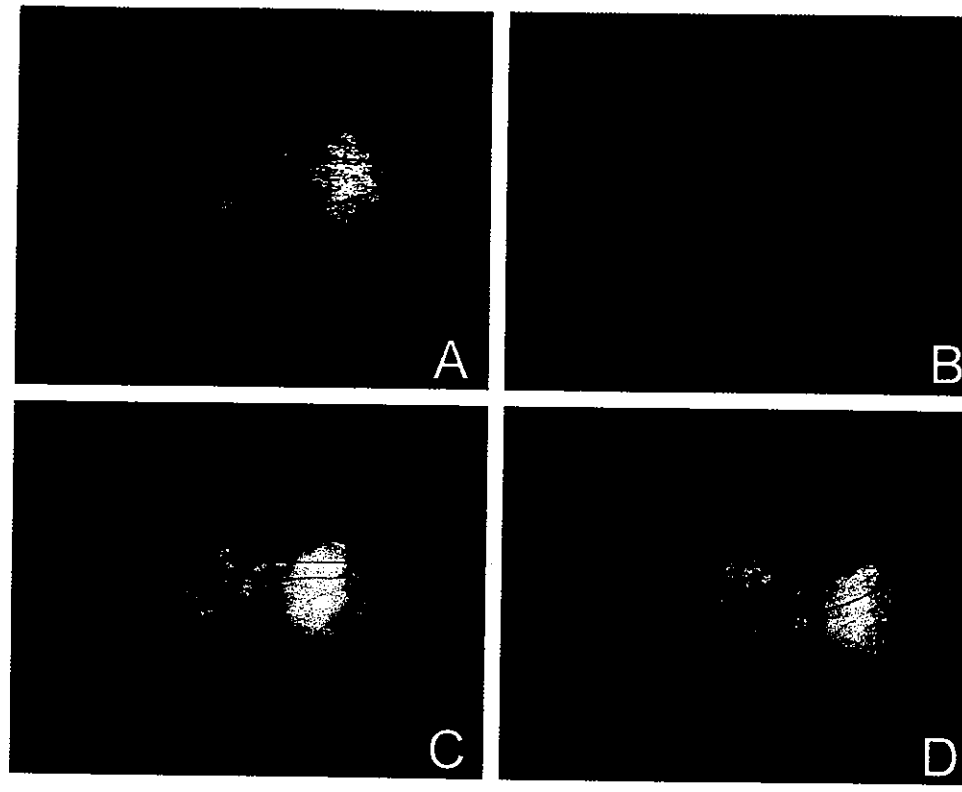

Fig. 1. Case 1. **A,** Preoperative photograph. A subfoveal CNV secondary to highly myopic degeneration is seen. Visual acuity was 20/200. **B,** Fluorescein angiography shows hyperfluorescence of the subfoveal CNV. **C,** Fundus photograph after MTSI. The macula is seen to be translocated inferiorly (arrow); the area where the CNV was removed is located extrafoveally (asterisk). The distance of translocation measures 1,190 μm. An inferior retinal fold extends from the optic disk (arrowheads) and moderate scleral infolding remains. **D,** Postoperative photograph after repair of retinal detachment. Two months after surgery for retinal detachment following MTSI, displacement of the fovea is 1,500 μm (arrow: foveal new location, asterisk: original foveal location) and the inferior retinal fold is not seen. Vision recovered to 20/200 from hand motion.

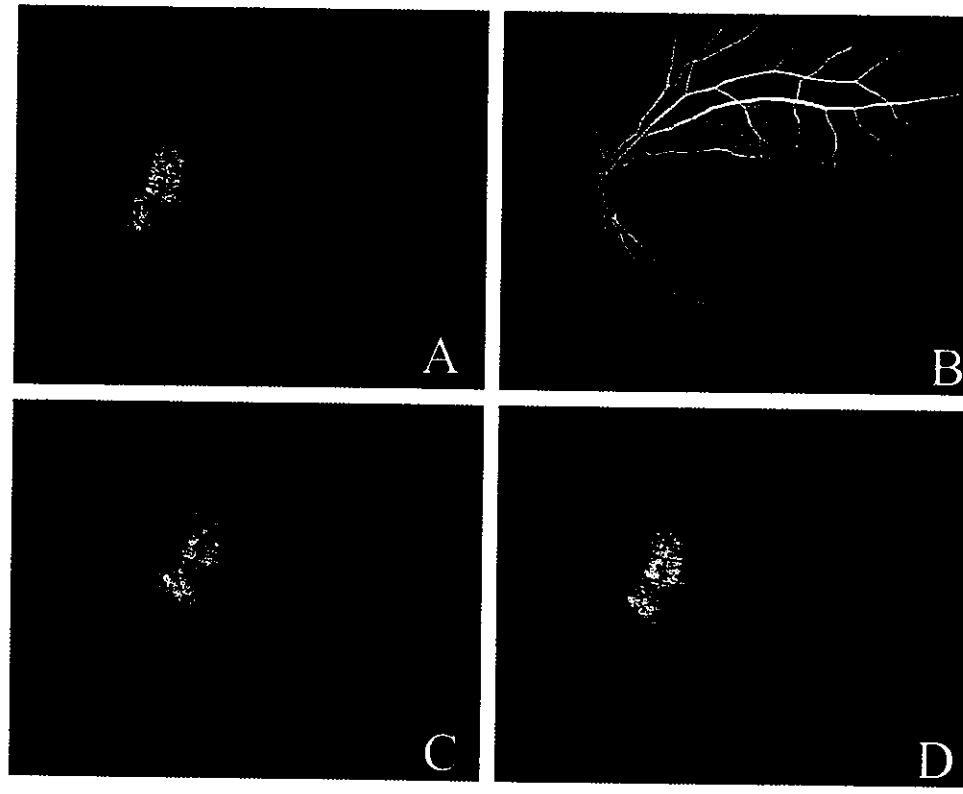

Fig. 2. Case 2. **A,** Preoperative photograph. A subfoveal CNV is seen. Visual acuity was 20/200. **B,** Fluorescein angiography shows hyperfluorescence of the subfoveal CNV. **C,** Postoperative photograph after MTSI. The macula is translocated inferiorly (arrow), and the area where CNV had existed is extrafoveal (asterisk). The distance of foveal displacement is 1,180 μm, although scleral infolding has disappeared rapidly. **D,** Postoperative photograph after repair of retinal detachment. Two months after retinal reattachment, displacement of the fovea is somewhat less 740 μm (arrow: foveal new location, asterisk: original foveal location). Vision recovered to 20/100 from hand motion.